JOURNAL OF CATALYSIS **179,** 565–580 (1998)
ARTICLE NO. CA982229

Platinum Clusters Supported in Zeolite LTL: Influence of Catalyst Morphology on Performance in *n*-Hexane Reforming

R. E. Jentoft,* M. Tsapatsis,† M. E. Davis,‡ and B. C. Gates*

*Department of Chemical Engineering and Materials Science, University of California, Davis, California 95616; †Department of Chemical Engineering, University of Massachusetts, Amherst, Amherst, Massachusetts 01003; ‡Chemical Engineering, California Institute of Technology, Pasadena, California 91125

Received February 25, 1998; revised June 16, 1998; accepted July 10, 1998

KLTL zeolite-supported platinum catalysts were synthesized from aqueous tetraammineplatinum(II) nitrate solutions and nonacidic KLTL zeolite crystallites, including some with dimensions as little as 300 × 500 Å. The zeolite crystallites had various morphologies, some being predominantly disk-shaped particles and some predominantly mosaics of rod-like domains with a range of *c*-dimension lengths. The activity and selectivity of each catalyst were evaluated for dehydrocyclization of *n*-hexane in the presence of H_2 to form predominantly benzene at conversions of typically 45–90%. The data presented here provide a detailed characterization of the deactivation of such catalysts in the absence of sulfur. EXAFS data show that the platinum in each catalyst was present in clusters of about 20 atoms each, on average. Electron micrographs show that the platinum clusters were nearly evenly dispersed on the surfaces of the zeolite crystallites, including the intracrystalline and extracrystalline surfaces. The catalytic performance was virtually independent of the zeolite channel length, but activity, selectivity, and resistance to deactivation were found to be correlated with the ratio of the surface area external to the crystallite domains to that within the intracrystalline pores. The catalyst performance is dependent on this ratio (which is related to the zeolite morphology) as follows: in comparison with the others, the catalysts with the relatively low fractions of platinum outside the intracrystalline pores are more active, more selective for benzene formation, and more resistant to deactivation. One well-prepared catalyst, for example, gave greater than 90% selectivity for benzene and no measurable deactivation over 140 h of operation in a flow reactor at 420°C and atmospheric pressure. These data match those characterizing the most selective catalysts reported. Consistent with the interpretation of E. Iglesia and J. E. Baumgartner (*in* "New Frontiers in Catalysis" (L. Guczi, F. Solymosi, and P. Tetenyi, Eds.), p. 993, *Studies in Surface Science and Catalysis,* Vol. 75. Elsevier, Amsterdam, 1993), catalyst deactivation is associated with platinum outside the zeolite pores; it is hypothesized that coke formation outside the pores is relatively rapid and that a distinguishing characteristic of the best catalysts is the presence of most of the platinum in the intracrystalline pores, where coke formation may be inhibited by the constraints of the pores.

INTRODUCTION

Platinum clusters in basic LTL zeolite are active, stable, and selective catalysts for the dehydrocyclization of straight-chain alkanes to give aromatics (1–4). An industrial process is carried out with such catalysts for the selective reforming of naphtha to give aromatics to be used as petrochemical intermediates (5). High selectivities have been observed with platinum on various nonacidic supports (6–9), and the best of the known catalysts for this process are platinum clusters supported in LTL zeolite. Reviews of this subject have appeared recently (10, 11), and critical assessments are included in the papers by Miller *et al.* (12) and McVicker *et al.* (13).

The reasons for the high dehydrocyclization selectivity of platinum supported on LTL zeolite are still not fully resolved. There is a consensus that the support must be nonacidic and that the catalyst is monofunctional, with platinum providing the catalytic sites. High selectivities for dehydrocyclization are associated with small clusters of platinum; these have been found to be as small as about 5–12 atoms in nuclearity (14).

Davis and Derouane (8) found that platinum supported on basic, high-surface-area magnesia-alumina was as active and selective as a sample of platinum supported on LTL zeolite, and Iglesia and Baumgartner (7) found that, prior to rapid deactivation during *n*-heptane conversion in the presence of H_2 (in the absence of sulfur), platinum supported on silica was as active as an LTL zeolite-supported catalyst. The results led these authors, and others (9–11), to emphasize the importance of the platinum cluster size.

Iglesia and Baumgartner (7) found that silica-supported platinum underwent much more rapid deactivation than their zeolite LTL-supported platinum, and they inferred that bimolecular self-poisoning reactions that led to deactivation of platinum on silica were not significant when the platinum was confined as clusters in the zeolite pores. This

0021-9517/98 $25.00

interpretation is supported by NMR results of Sharma *et al.* (15) for CO adsorbed on platinum in each of the two types of catalyst. These results are consistent with the attribution of the high selectivities of the zeolite LTL-supported catalysts to a high intrinsic selectivity combined with stability of platinum clusters confined in the zeolite LTL pores.

Miller *et al.* (12), agreeing with the importance of the small platinum cluster size and the need for a nonacidic support, concluded that part of the reason for the high selectivity of platinum in LTL zeolite for *n*-hexane dehydrocyclization at 420°C is the unique geometry of the LTL zeolite pores, whereby the adsorbed *n*-hexane is presumably aligned in the pore in a manner that favors 1–6 ring closure in the alkane (consistent with the earlier suggestion of Derouane and Vanderveken (16)). Miller's evidence for this geometric effect is his experimental ratios of the rate of 1–6 ring closure to the rate of 1–5 ring closure at about 10% conversion of *n*-hexane in the presence of catalysts consisting of highly dispersed platinum on various supports, characterized by hydrogen chemisorption (12). This ratio was found to be about 1.3 when the support was zeolite LTL and substantially less when the supports were other zeolites or mesoporous solids. On the other hand, Mielczarski *et al.* (9), who made measurements similar to those of Miller *et al.* (12), but at a higher temperature (460°C), observed dehydrocyclization selectivities at conversions of about 15% that did not depend on the pore structure of the various zeolites and mesoporous solids; these authors concluded that the platinum dispersion (characterized by hydrogen chemisorption) and not the pore size was important in affecting the selectivity.

There are only a few reports of deactivation of LTL zeolite-supported platinum catalysts, and almost all are concerned with deactivation in the presence of sulfur. Hughes *et al.* (3) reported the sensitivity of the catalyst to sulfur poisoning, and McVicker *et al.* (13) presented data illustrating the rapid catalyst deactivation caused by sulfur poisoning. The latter authors concluded that sulfur compounds caused migration of the platinum to form clusters large enough to block the zeolite pores and thus isolate the platinum within them. They found that regeneration gave catalysts with increased resistance to sulfur poisoning (17), but regeneration did not lead to full recovery of the activity. Vaarkamp *et al.* (18) found that exposure of the catalyst to sulfur increased the platinum cluster nuclearity from about 6 atoms to about 13 atoms, on average; the 13-atom clusters, if spherical, would be approximately 8 Å in diameter, large enough to block the zeolite pores.

Our objectives were to prepare and characterize highly dispersed Pt/LTL zeolite catalysts by using zeolite crystallites of relatively well-defined morphology and size and to determine how the morphology and preparation methods affect the catalytic activity, selectivity, and stability in *n*-hexane conversion in the absence of sulfur. Various batches of LTL zeolite crystallites were prepared, with most of the crystallites being extremely small and offering the prospect of good characterization by transmission electron microscopy (TEM) to allow determination of the distribution of platinum inside and outside the pores. The platinum clusters were characterized by extended X-ray absorption fine structure (EXAFS) spectroscopy, and the catalyst performance was determined for high conversions of *n*-hexane in H_2 at 420°C. The data reported here are the first giving detailed evidence of the deactivation of LTL zeolite-supported platinum catalysts for alkane dehydrocyclization in the absence of sulfur.

EXPERIMENTAL METHODS

Catalyst Preparation

One of the samples of LTL zeolite (Sample 1, Table 1) was provided by Miller; it is similar to samples described in his work (6, 12). Other zeolite samples were synthesized as described elsewhere (19). Each zeolite was calcined in air at 590°C for 2 h.

The platinum precursor was tetraammineplatinum nitrate (Strem, 99%). Small amounts of each zeolite sample (0.14–1.5 g) were impregnated with an aqueous solution of the precursor by the incipient wetness method. Each impregnated sample was dried at room temperature under vacuum for 1 h, calcined in air at 260°C for 3 h, and reduced in flowing H_2 at 500°C for 1 h (60 cm^3/min, 1 atm). One of the samples (Sample 3, Table 1) was treated with additional KCl, added after the zeolite had been neutralized (by washing to a pH of 7) and prior to the addition of platinum. Table 1 is a summary of the catalyst samples with the notation used to designate them and details of the synthesis and characterization.

Catalytic Reactions

The catalytic conversion of *n*-hexane (Aldrich, 99.3%, with impurities of 0.6 wt% methylcyclopentane (MCP) and 0.1 wt% 3-methylpentane) was carried out at atmospheric pressure in a once-through stainless-steel flow reactor at 420°C. H_2 (99.99999%) was formed by electrolysis of water in a Balston 75-33 H_2 generator and flowed through traps containing activated 4A molecular sieve and MnO. Catalyst particles (100–250 mg) were mixed with inert α-Al_2O_3 particles in a mass ratio of 1 : 1. Prior to reaction, the catalyst was reduced in flowing H_2 at 500°C for 1 h and then cooled to the reaction temperature in flowing H_2. Liquid *n*-hexane feed flowed from an ISCO 260D pump to a vaporizer held at 140°C, where it was mixed with H_2. The H_2 and *n*-hexane flow rates were adjusted to give a H_2 : *n*-hexane molar ratio of 7.8 : 1.

TABLE 1

List of Catalysts and Details of Synthesis

Sample number	Preparation				Techniques used to determine crystallite morphology and dimensions	*c*-Direction dimension of crystallites (Å)	Zeolite morphology	Extracrystalline to intracrystalline surface area ratio
	Composition of synthesis mixtur $K_2O : Al_2O_3 : SiO_2 : H_2O$	g Pt/ g soln	g soln/ g zeolite	Pt content, wt%				
1[a]	10 : 1 : 25 : 400	—	—	1.2	TEM	500–3000	well developed cylinders	smallest
2	10 : 1 : 25 : 400	1.1	0.0077	0.85	TEM and XRD line broadening of [001] peak	200	disk-like crystallites 1000 Å diameter; same as Sample 3 after addition of KCl	small
3	10 : 1 : 25 : 400 (before addition of KCl)	0.8	0.0104	0.83	TEM and XRD line broadening of [001] peak	200	disk-like crystallites 1000 Å diameter; same as Sample 2 before addition of KCl	small
4	10 : 1 : 20 : 1000	1.17	0.0075	0.88	TEM and SEM	1000–5000	mosaic crystals with 1000–5000 Å grains	small/ intermediate
5	10 : 1 : 20 : 600	1.16	0.0075	0.86	TEM	300–600	mosaic crystals consisting of aligned cylindrical grains	intermediate
6	10 : 1 : 20 : 400	0.77	0.0104	0.80	TEM and XRD line broadening of [001] peak	300	mosaic crystals consisting of aligned nanocrystalline grains (300 × 150 Å)	largest
7	10 : 1 : 20 : 400	1.19	0.0063	0.75	TEM and XRD line broadening of [001] peak	300	mosaic crystals consisting of aligned nanocrystalline grains (300 × 150 Å)	largest

[a] Sample provided by Miller and similar to that of Lane *et al.* (6).

The reaction products were analyzed with an on-line Hewlett Packard 5890 Series II gas chromatograph with a flame ionization detector and a J&W alumina PLOT column 0.53 mm in diameter and 30 m long. All the major products were separated in the column, except for cyclohexane and MCP, which co-eluted.

Because the catalyst samples had different platinum contents (in the range of 0.8–1.2 wt%), the data were normalized by using values of weight hourly space velocity (WHSV) based on mass of platinum; WHSV varied from 125 to 3920 g of *n*-hexane/(g of Pt · h).

Catalyst Characterization

Transmission electron microscopy. Samples were characterized with a Philips 430 microscope operated at 200 kV and with a Jeol ARM-1000 microscope operated at 800 kV. Energy dispersive X-ray (EDX) microanalysis was performed on a Jeol Jem 200 CX AEM instrument equipped with a KEVEX high-angle energy dispersive X-ray detector. Most of the micrographs and all the EDX spectra were recorded by using a liquid nitrogen-cooled stage to minimize sample damage; high-resolution images were recorded with 1-s exposures and the total time in the beam was kept less than 5 s; thus, it is believed that no substantial changes of the platinum clusters resulted from beam damage.

EXAFS spectroscopy. Data were collected at beam line X-11A at the National Synchrotron Light Source at Brookhaven National Laboratory, Upton, New York. The storage ring operated with an electron energy of 2.5 GeV and a current of 170–220 mA. The Si(111) double crystal monochromator was detuned by 20% to minimize higher harmonics in the X-ray beam. The samples were pressed into self-supporting wafers and placed into a cell which allowed treatment in flowing gases prior to measurement (20). Data were collected at the Pt L_{III} edge (11564 eV) with the sample under vacuum and cooled to nearly liquid

nitrogen temperature. The fresh catalyst samples were reduced at various temperatures in flowing H_2 (Matheson 99.999%) prior to data collection. The data were acquired in the transmission mode and integrated for 1 s at each energy in the range from 200 eV below the absorption edge to 975 eV beyond the edge.

A sample of catalyst that had been used in the flow reactor was transferred under N_2 to the EXAFS cell, treated in flowing H_2 at 500°C and 1 atm for 1 h, and then evacuated and scanned.

EXAFS reference data. The EXAFS data characterizing the zeolite LTL-supported platinum catalysts were analyzed by using experimentally and theoretically determined reference data. The experimental references were obtained from materials of known structure. The Pt-Pt and Pt-O interactions were measured by using platinum foil and $Na_2Pt(OH)_6$, respectively, with reported parameters (21). Pt-Si, Pt-Al, Pt-K, and Pt-C interactions were modeled with the FEFF-4 software of Rehr *et al.* (22).

EXAFS DATA ANALYSIS

The data from six scans for each of the Pt/KL TL zeolite catalysts characterized by this method were averaged and analyzed with the XDAP software (23) to estimate the parameters that characterize the high-Z (Pt) and low-Z (O) contributions by multiple-shell fitting in k space (k is the wave vector) and in r space (r is the distance from the absorbing atom, Pt). The EXAFS contributions were determined by applying the difference file technique to phase- and amplitude-corrected Fourier transforms (24). The fit parameters characterizing the Pt and O contributions were optimized with both k^1 and k^3 weighting to avoid overemphasizing or underemphasizing either the high-Z (Pt-Pt) or low-Z (Pt-O) contributions.

Once a good fit had been obtained to estimate the EXAFS parameters N, $\Delta\sigma^2$, R, and ΔE_0 (where N is the coordination number, $\Delta\sigma^2$ the Debye–Waller factor, R the Pt-backscatterer distance, and ΔE_0 the inner potential correction) with k^1 and k^3 weightings, the fit was optimized by allowing a few of the parameters to be fitted while the other were held fixed. As a final step in the optimization, additional small contributions were added to the total fit to determine their effect on the larger Pt-Pt and Pt-O contributions. These small contributions are not reported explicitly; they were used only to test their influence on the larger contributions and to ensure that the fitted contributions remained within the reported error bounds.

The number of parameters used to fit the data was limited to at most the statistically justified number, n, calculated from the Nyquist theorem (25) ($n = 2\Delta k \Delta r/\pi + 1$, where Δk and Δr are the ranges used to fit the data in k and in r space, respectively).

RESULTS

Transmission Electron Microscopy

Images of catalyst samples supported on LTL zeolite crystallites are shown in Fig. 1. The zeolite particles are classified roughly into three groups, namely, disks (Samples 2 and 3), large mosaic crystals (Samples 4 and 5), and smaller mosaic crystals (Samples 6 and 7) which have been reported elsewhere (26). The disks of Samples 2 and 3 were typically about 200 Å long and 1000 Å in diameter. The crystallite c-axis (the axis parallel to the channels) was oriented along the 200-Å length. The rod-shaped crystallites of Samples 6 and 7 were typically 200–300 Å long (along the c-axis) and approximately 150 Å in diameter. These crystallites formed a mosaic tertiary structure. The rods tended to align with each other and form small clusters which were also roughly cylindrical in shape, consisting usually of <10 rods per cluster (19). The small clusters of rods forming the particles of Samples 6 and 7 were stable under the conditions used to impregnate the zeolite with platinum. The mosaic crystallites of Samples 4 and 5 were characterized by a morphology similar to that of Samples 6 and 7, but with larger rod and crystallite sizes. The catalyst investigated by Lane *et al.* (6) and Sample 1 of this work were rounded or rectangular crystallites with lengths of roughly 500–3000 Å.

The surface areas of the crystallites are categorized into an intracrystalline fraction and an extracrystalline fraction, the latter corresponding to surfaces not isolated by the approximately 7.1-Å restriction of the zeolite pore channel. The extracrystalline fraction includes the particle exteriors and the surfaces between the crystal domains. Some of the zeolite crystal domains were so small that the external area was a significant fraction of the total area. The diameters of the pores between the domains were found to range from the intracrystalline zeolite pore diameter to the domain size.

The TEM images allow a qualitative grouping of the catalyst samples on the basis of the ratio of external surface area to intracrystalline surface area. The catalyst samples are numbered (Table 1) in order of increasing ratio of extracrystalline to intracrystalline surface area; the ratios were found to be about the same for Samples 2 and 3 and for Samples 6 and 7.

The samples were examined at high magnification after impregnation and reduction at 500°C, and several were also examined after use as catalysts. The TEM images lead to the following observations about the fresh and used catalysts: the relatively large zeolite LTL particles in Samples 1 and 4 gave no indication of contrast in the TEM images that could be interpreted as evidence of platinum clusters or particles. Microtomy was not attempted for Samples 1 and 4, but Sample 1 was examined by EDX, as described below. The remaining samples consisted of thin zeolite crystallites,

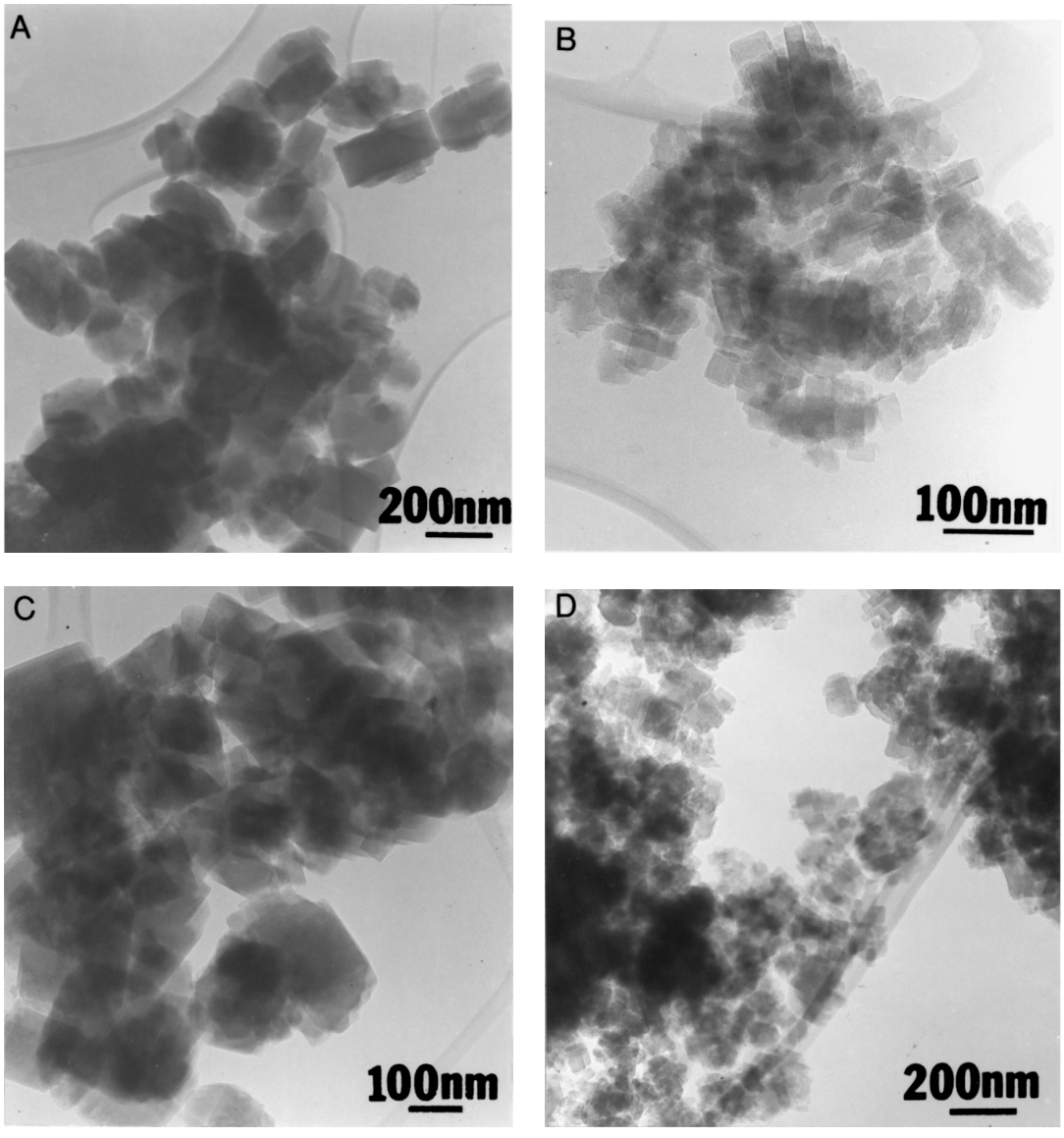

FIG. 1. Transmission electron micrographs of catalyst samples: A, Sample 1, 500–3000 Å cylinders; B, Sample 2, disk-like crystallites; C, Sample 4, large grain mosaics; D, Sample 5, large grain mosaics.

in which numerous small scattering centers were observed, which are interpreted as evidence of platinum clusters and particles.

Beam damage occurred during the TEM experiments, but observations made in the early stages are believed to characterize virtually unperturbed samples. The images indicate that the contrast attributed to platinum clusters extended into regions smaller than those characterized by the contrast associated with the 12-membered zeolite ring openings or fringe spacings, suggesting the presence of platinum clusters smaller than about 10 Å in diameter; the location of the platinum was within 12-membered ring channels, as shown in Fig. 2, where views down the *c*-crystallographic direction and perpendicular to the *c*-crystallographic direction are presented for Samples 2, 5, and 6. No preferential location of the platinum was indicated by the microscopic data. Platinum appeared to be randomly distributed throughout the intracrystalline pores as well as on the external surfaces; the data do not allow a distinction between the sizes of the platinum clusters supported on the extracrystalline surfaces and those supported on the intracrystalline surfaces. Equivalent results were obtained for Sample 1 by EDX analysis in the STEM with a 100-Å beam. About 10 spots were analyzed in three zeolite crystals, and no preferential location of platinum was indicated.

Prolonged observation of the catalyst samples led to the breakup of the zeolite lattice by the beam and to the appearance of platinum clusters and particles with contrast

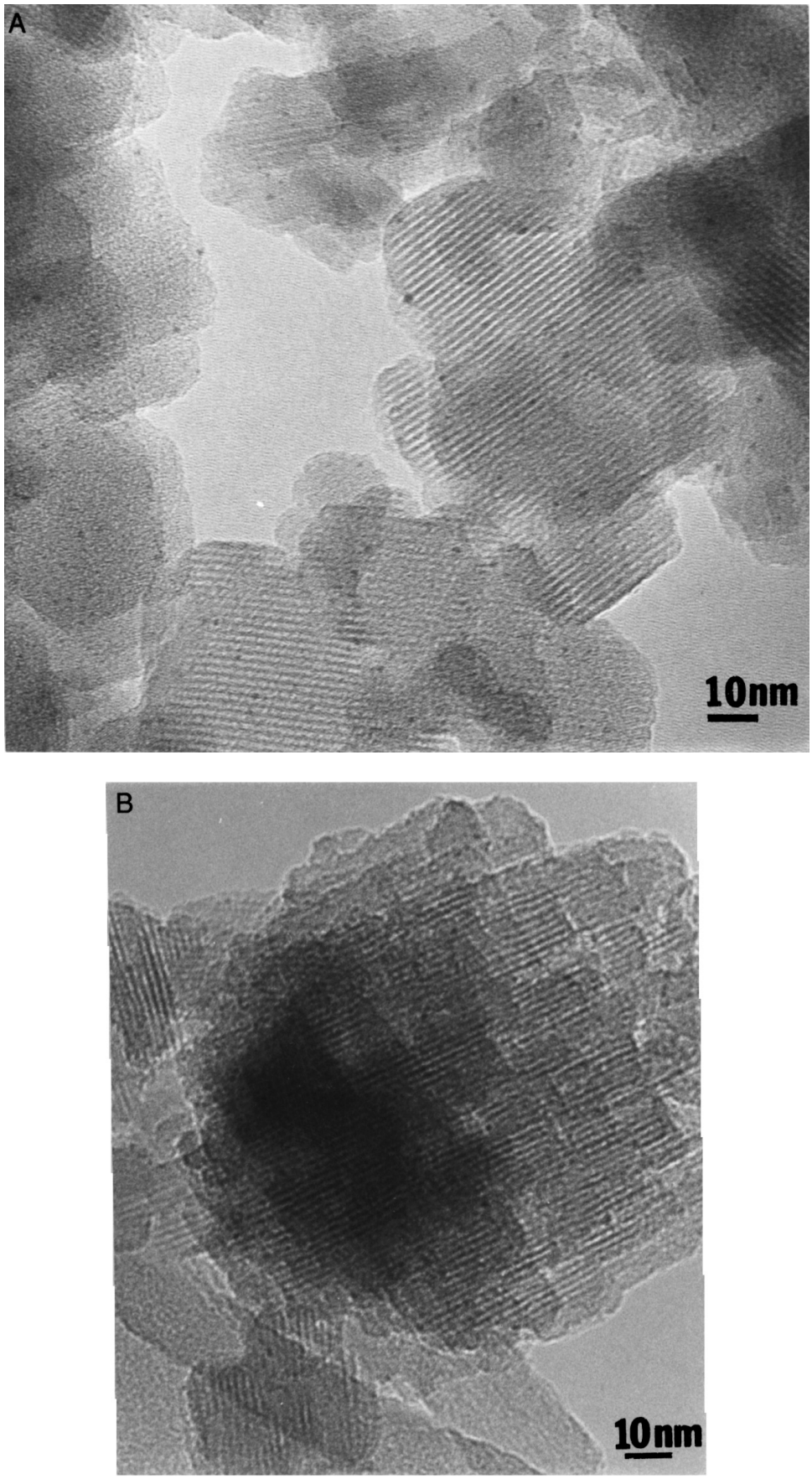

FIG. 2. Transmission electron micrographs of catalyst samples showing contrasts attributable to platinum clusters between fringe spacings of 18.4 Å: A, Sample 2; B, Sample 6; C, Sample 5.

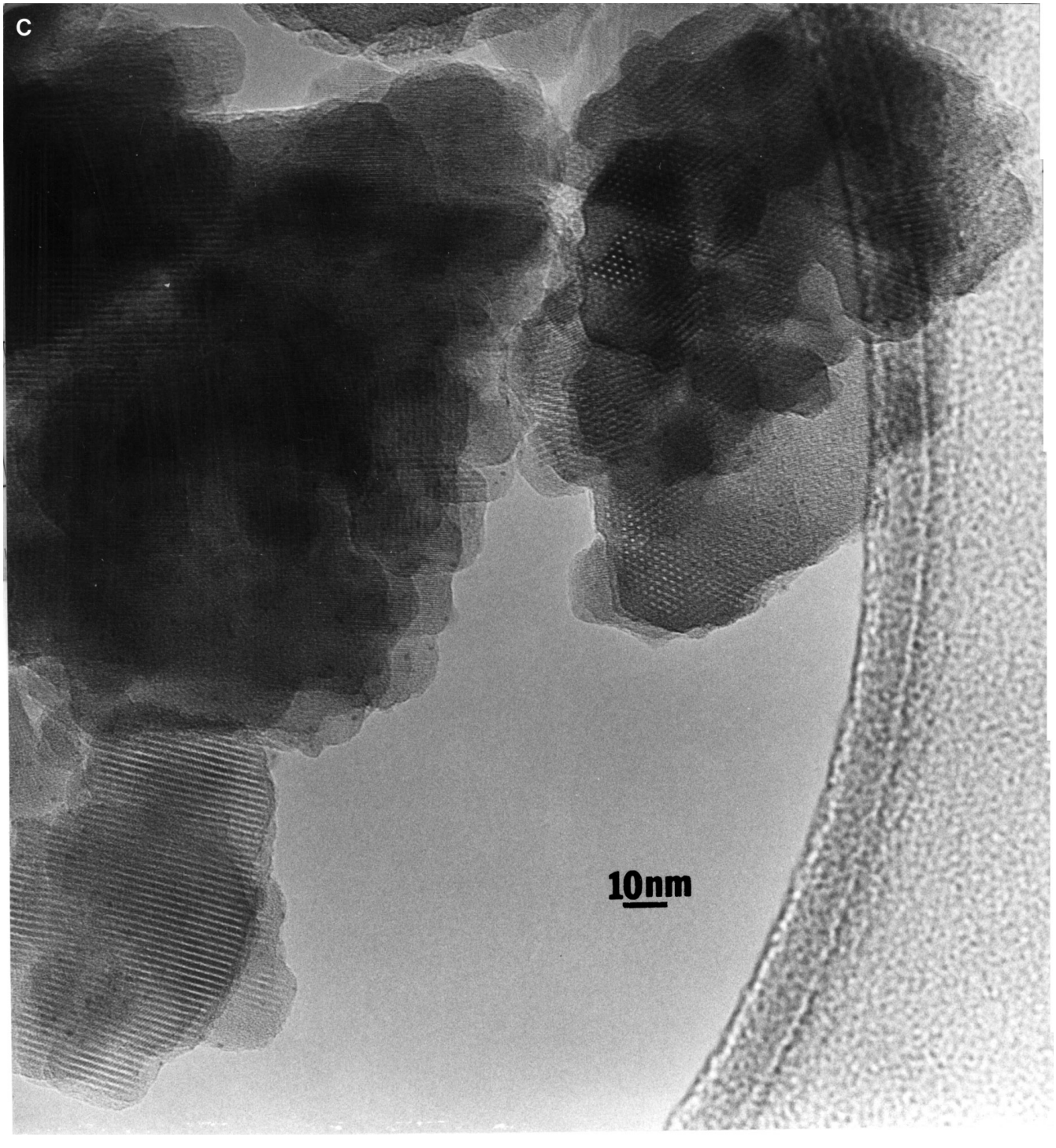

extending into regions larger than the zeolite unit cell. It is evident that platinum migration and agglomeration took place during the destruction of the zeolite framework, as expected (27).

EXAFS Spectroscopy

The raw EXAFS data characterizing Sample 3, reduced in H_2 at 300°C for 1 h, were Fourier filtered from 3.60 to

TABLE 2

EXAFS Data Characterizing Fresh and Used Pt/LTL Zeolite Catalysts[a]

Catalyst sample number	Treatment	Backscatterer	N	R, Å	$\Delta\sigma^2$, Å^2	ΔE_0, eV
1	H_2, 300°C, 1 h	Pt	5.06 ± 0.12	2.667 ± 0.002	0.0104 ± 0.0003	-4.73 ± 0.18
		O	1.67 ± 0.03	2.078 ± 0.002	0.0009 ± 0.0002	-1.50 ± 0.20
		O	1.55 ± 0.04	2.641 ± 0.003	0.0002 ± 0.0004	9.12 ± 0.31
1	H_2, 300°C, 1 h	Pt	5.56 ± 0.07	2.721 ± 0.001	0.0046 ± 0.0001	-3.24 ± 0.17
	then 500°C, 1 h	O	1.07 ± 0.05	2.090 ± 0.005	0.0082 ± 0.0008	-0.60 ± 0.58
		O	0.83 ± 0.02	2.725 ± 0.003	-0.0018 ± 0.0003	-2.36 ± 0.38
3	H_2, 300°C, 1 h	Pt	4.49 ± 0.01	2.74 ± 0.001	0.0028 ± 0.0001	0.60 ± 0.26
		O	1.54 ± 0.04	2.62 ± 0.004	0.0009 ± 0.0004	7.73 ± 0.55
3	H_2, 300°C, 1 h	Pt	5.36 ± 0.12	2.743 ± 0.001	0.0033 ± 0.0001	-0.54 ± 0.26
	then 500°C, 1 h	O	0.32 ± 0.04	2.143 ± 0.005	-0.0024 ± 0.0008	-14.96 ± 0.95
		O	1.70 ± 0.11	2.616 ± 0.006	-0.0023 ± 0.0060	11.42 ± 1.02
6	H_2, 300°C, 1 h	Pt	5.04 ± 0.10	2.742 ± 0.001	0.0027 ± 0.0002	-1.37 ± 0.15
		O	0.17 ± 0.03	2.17 ± 0.02	-0.005 ± 0.002	-1.1 ± 4.4
		O	1.08 ± 0.26	2.49 ± 0.01	-0.001 ± 0.002	17.7 ± 1.3
6	H_2, 300°C, 1 h	Pt	4.86 ± 0.14	2.742 ± 0.001	0.0034 ± 0.0001	-2.86 ± 0.07
	then 500°C, 1 h	O	0.93 ± 0.03	2.197 ± 0.003	0.0024 ± 0.0005	-13.80 ± 0.26
		O	0.45 ± 0.04	2.718 ± 0.007	-0.0003 ± 0.0006	-6.85 ± 0.85

[a] Notation: N, Pt-backscatterer coordination number; R, distance from Pt to backscatterer; $\Delta\sigma^2$, Debye–Waller factor; ΔE_0, inner potential correction.

15.88 Å^{-1} in k space, and then from 1.31 to 4.11 Å in r space. The k^3-weighted, filtered EXAFS data (the average of six scans) and the best fit are shown in Fig. 3A. The Fourier transform of these data (k^3 weighted) and the Fourier transform of the best fit are presented in Fig. 3B; these show good agreement with each other between values of r of 1.8 and 3.0 Å. The representation of the residual remaining after subtraction of the fit from the filtered EXAFS data is presented in Fig. 3C. The standard deviation representing the data scatter in the six spectra (Fourier filtered) which were averaged prior to analysis (Fig. 3C) is of the same magnitude as the residual, indicating that the fit represents the data to within twice the standard deviation of the six scans. These data were fitted with two shells, Pt-Pt and Pt-O. Figures 3D and 3E show the Fourier transform representations of these shells.

Using the result of the Nyquist theorem ($n = 2\Delta r \Delta k/\pi = 18.4$) to estimate the number of parameters n that can be statistically justified to determine a fit with these data, we infer that four shells is the maximum justified number. Thus, an alternative fitting was carried out with four shells, a Pt-Pt shell, two Pt-O shells, and a Pt-Si shell. The addition of the second Pt-O shell and the Pt-Si shell improved the overall fit only slightly, and because the contributions of the additional shells were of the order of the noise in the data, they are regarded as insignificant and not presented here. The fitting of the data with up to four shells did, however, provide a basis for estimating the effect of these small contributions on the Pt-Pt coordination number. The range of Pt-Pt coordination numbers obtained by fitting from two to four shells was 4.2 to 4.9, which corresponds to a deviation of only less than 10% from the coordination number of 4.5 that was obtained with the best two-shell fit. The EXAFS parameters determined in the preferred two-shell fit are summarized in Table 2.

EXAFS data were also obtained characterizing fresh catalyst Sample 3 after an additional reduction in H_2 at 500°C and Samples 1 and 6 after reduction in H_2 at 300°C and again after an additional reduction in H_2 at 500°C. The method of data analysis is as described above for Sample 3. The EXAFS parameters are summarized in Table 2. The data characterizing each sample indicate a strong Pt-Pt contribution with a distance R of about 2.7 Å with a Pt-Pt coordination number of about 5.1, corresponding to an average platinum cluster nuclearity of approximately 20 atoms and an average diameter of about 7 Å (28). The Debye–Waller factor characterizing the Pt-Pt shell in each sample was found to be relatively large (Table 2), which indicates a substantial variation in the Pt-Pt distances, possibly indicating a relatively nonuniform distribution of cluster structures. In addition to the Pt-Pt contribution, a Pt-O contribution was found for each sample, with a Pt-O distance of about 2.6 Å. With the exception of Sample 3 after the first reduction at 300°C, the data indicated an additional Pt-O contribution at about 2.1 Å.

Catalyst Performance

The major reaction products formed from *n*-hexane in the presence of H_2 at 420°C were benzene, cyclohexane/MCP,

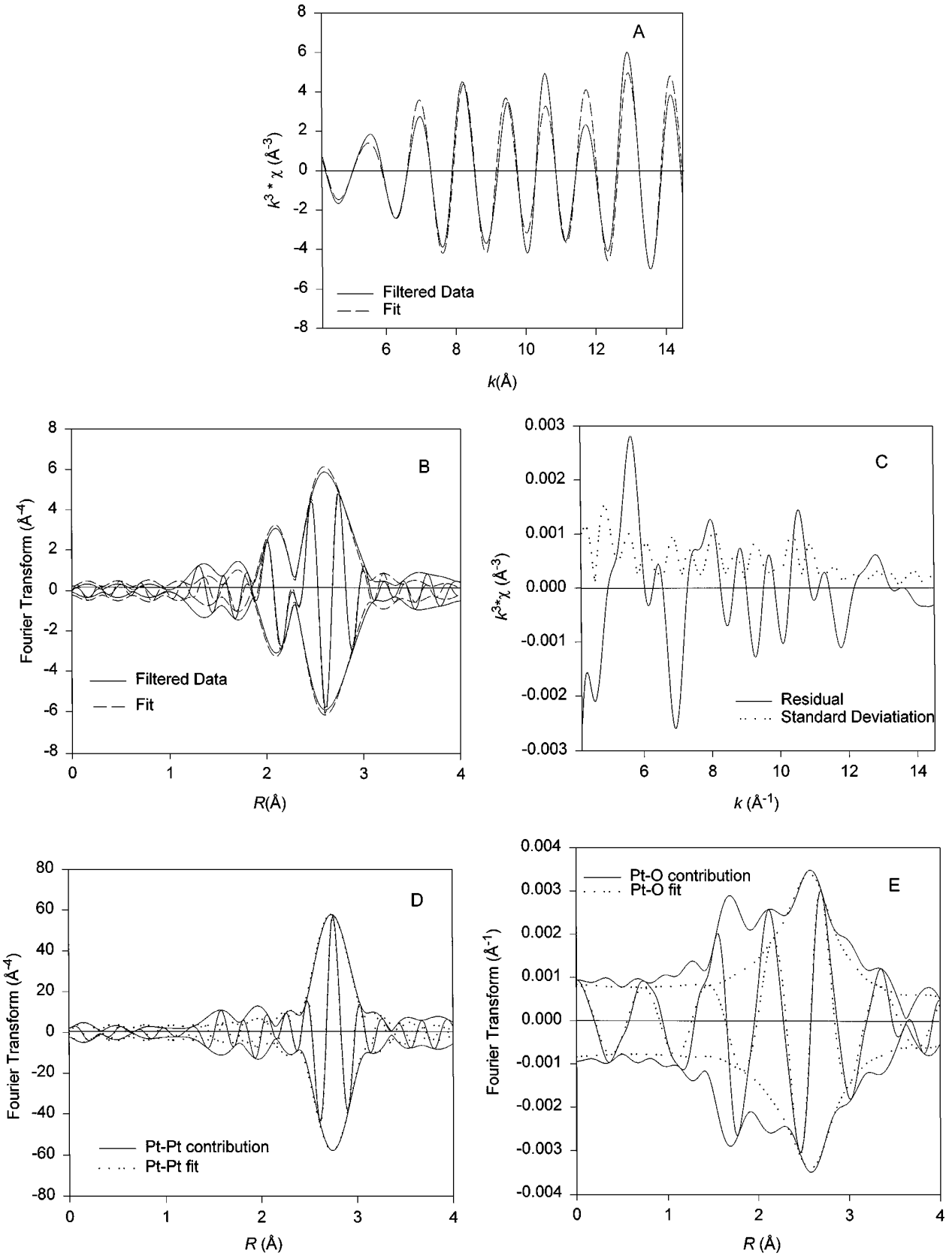

FIG. 3. Results of EXAFS analysis characterizing Pt/KLTL zeolite Sample 3 after 1 h in H_2 at 300°C: A, chi (EXAFS function) representation, k^3-weighted; B, Fourier transform representation, k^3-weighted; C, chi standard deviation and residual; D, Fourier transform of Pt-Pt shell, k^3-weighted; E, Fourier transform of Pt-O shell, k^1-weighted.

methylpentanes, and C_{1-5} hydrocarbons (hydrogenolysis products), in agreement with earlier reports; no alkene products were observed. Catalyst Sample 1, which is virtually the same as those reported earlier (6, 29, 30), was tested over a range of space velocities under conditions matching those of Lane *et al.* (6). The product distribution data (which are similar to those of Lane *et al.* (6)) show that the concentrations in the product of benzene and of C_{1-5} hydrocarbons increased with increasing *n*-hexane conversion and that the concentrations in the product of methylpentanes and of cyclohexane/MCP passed through maxima at *n*-hexane conversions of 0.8 and 0.5, respectively.

The conversion data shown in Fig. 4A indicate the stability of the catalysts during operation in the flow reactor. Catalyst Samples 1, 2, and 3 maintained total *n*-hexane conversions >90% during operating periods of up to 140 h; these catalysts hardly lost any activity during this operation. In contrast, the other catalysts lost substantial activity (Table 3). The trends in the total conversion of *n*-hexane (Fig. 4A) are similar to the trends in the conversion of *n*-hexane to benzene (Fig. 4B). Catalyst Samples 1 and 2 gave low and nearly constant conversions to C_{1-5} products (0.04 and 0.06, respectively) (Fig. 4C). Catalyst Sample 3 gave a similarly low (0.06) but slightly decreasing conversion to C_{1-5} hydrocarbons, and catalyst Sample 6, tested at a higher space velocity, gave a low but decreasing conversion to C_{1-5} hydrocarbons. The remaining catalysts gave much higher initial conversions to these products with rapidly decreasing conversions that stabilized at about 0.08 after 20 to 40 h on stream.

The product distribution data (Figs. 5A–C) show that benzene was the major product, with the benzene selectivity, defined as moles of benzene produced/mole of *n*-hexane converted, being between 0.60 and 0.91 for all catalysts for all times on stream (Fig. 5A). The benzene selectivity was highest and remained nearly constant for catalyst Samples 1 and 2. Catalyst Samples 3, 4, and 5 gave slightly lower benzene selectivities that decreased slightly with increasing

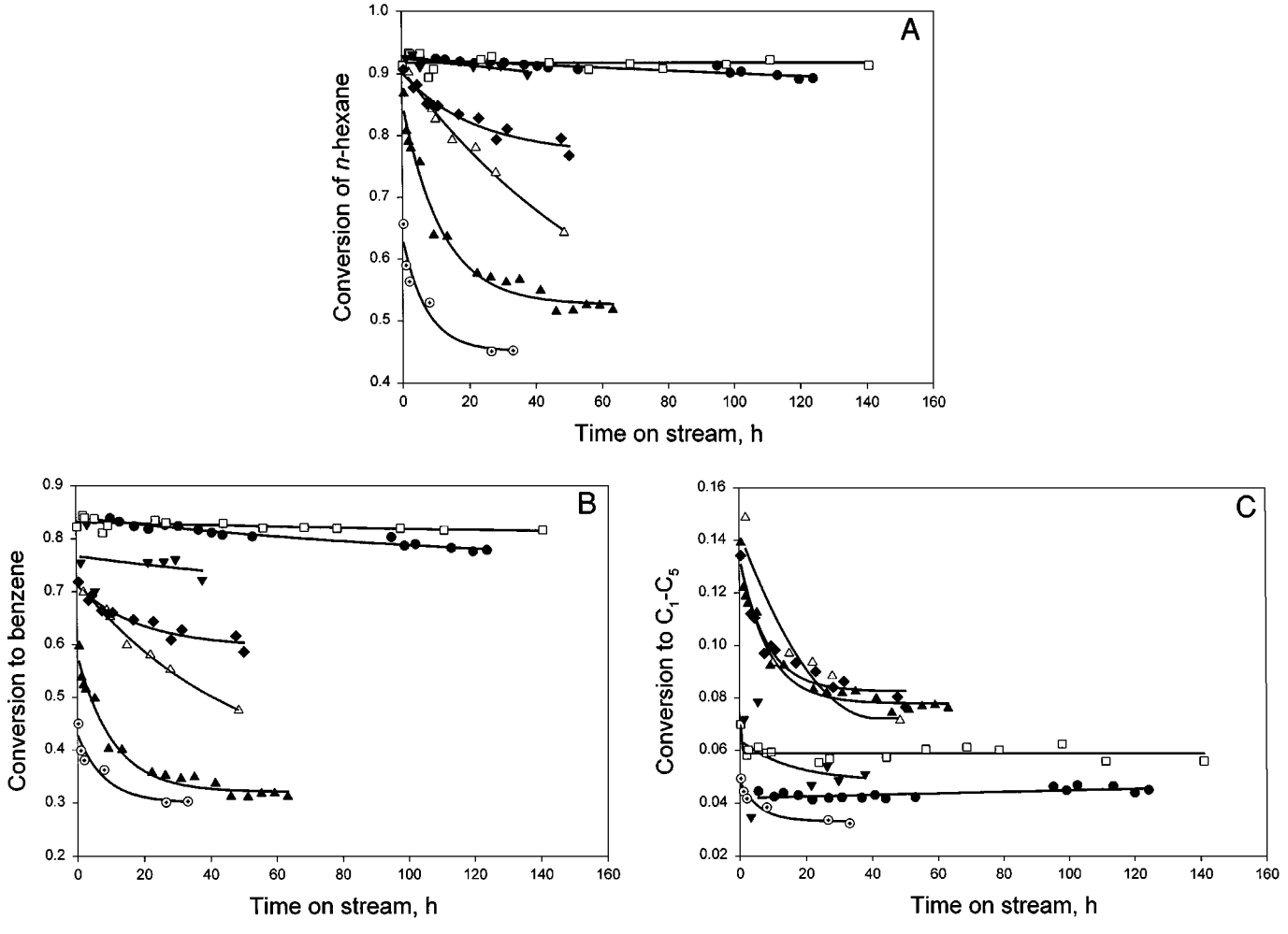

FIG. 4. Deactivation of Pt/KLTL zeolite catalyst in *n*-hexane conversion at 420°C: A, *n*-hexane; B, benzene; C, C_1–C_5. Symbols: ●, Sample 1; □, Sample 2; ▼, Sample 3; ◆, Sample 4; △, Sample 5; ⊙, Sample 6; ▲, Sample 7.

TABLE 3

Rates of Catalyst Deactivation, Represented in Terms of Decline in Conversion to Benzene with Time on Stream

Catalyst sample number	WHSV, g of *n*-hexane/(g of Pt · h)	Rate of deactivation averaged over 30 h onstream,[a] h^{-1}	Rate of deactivation extrapolated to zero time on stream,[b] h^{-1}	Extacrystalline to intracrystalline surface area ratio
1	144	0.0006 ± 0.0003	0.001	Smallest
2	145	0.0002 ± 0.0003	0.000	Small
3	143	0.0008 ± 0.0003	0.001	Small
4	142	0.0031 ± 0.0003	0.006	Small/intermediate
5	146	0.0059 ± 0.0003	0.008	Intermediate
7	139	0.0065 ± 0.0003	0.025	Largest
6	504	0.0042 ± 0.0003	0.016	Largest

Note. Qualitative external/internal surface area ratios and *c*-direction crystallite length were determined from TEM data. Reaction conditions for all catalysts were H_2/HC molar ratio = 7.8; temperature = 420°C.

[a] Defined as magnitude of change in conversion to benzene/time on stream, averaged over the first 30 h on stream; mol benzene/mol *n*-hexane h.

[b] Defined as magnitude of change in conversion to benzene/time on stream extrapolated to zero time on stream.

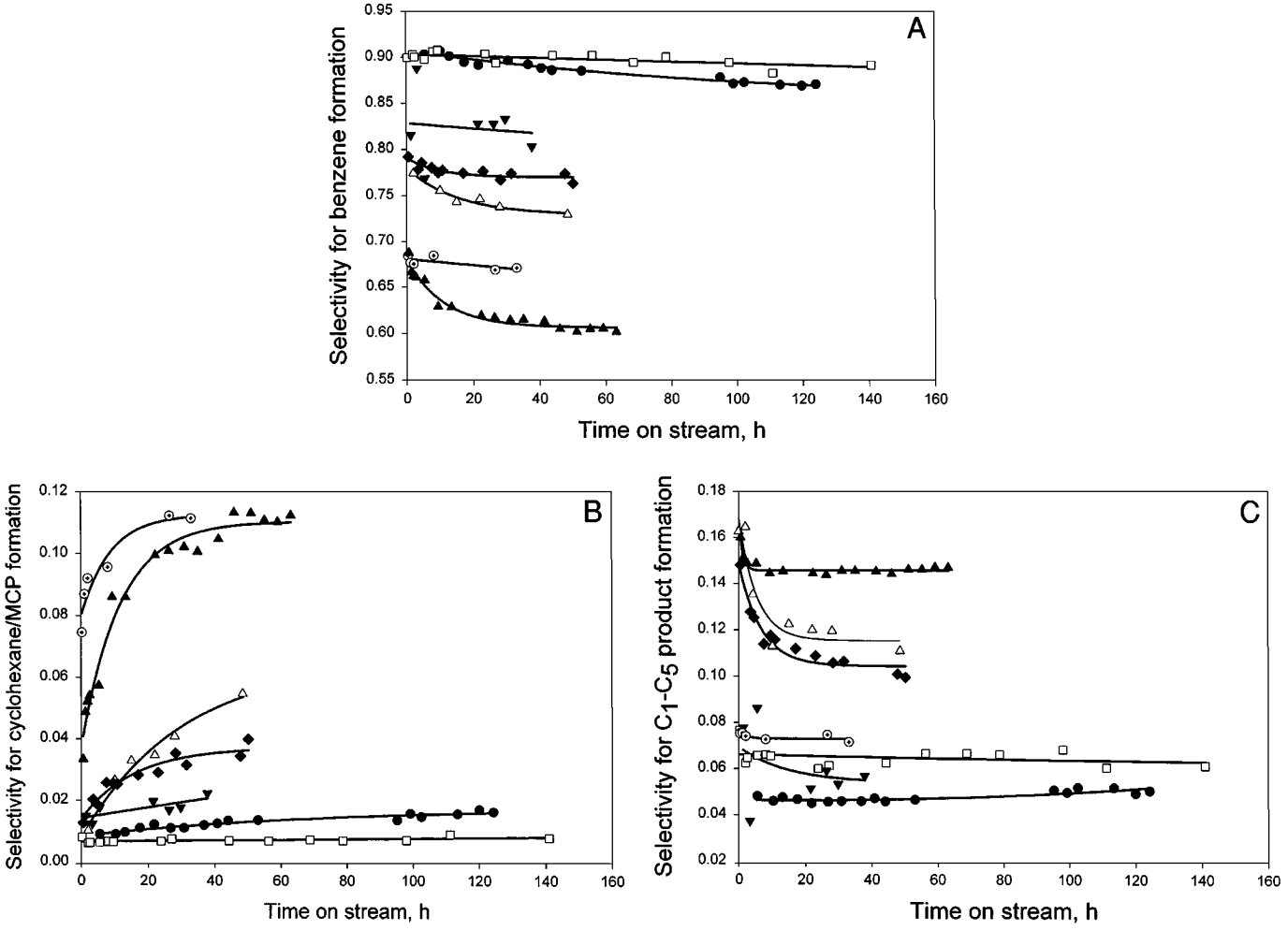

FIG. 5. Changes in selectivity of products during operation of Pt/KLTL zeolite catalyst in *n*-hexane conversion at 420°C: A, benzene; B, cyclohexane/MCP; C, C_1-C_5. Symbols: ●, Sample 1; □, Sample 2; ▼, Sample 3; ◆, Sample 4; △, Sample 5; ⊙, Sample 6; ▲, Sample 7.

TABLE 4

Initial *n*-Hexane Conversion Data and Product Selectivities for the Reaction Catalyzed by Pt/LTL Zeolite

Catalyst sample	*n*-Hexane conversion	Benzene selectivity[a]	C_1-C_5 selectivity[a]	Cyclohexane/MCP selectivity[a]	Methylpentane selectivity[a]	*c*-Direction crystallite length, Å
1	0.92	0.91	0.05	0.01	0.04	500–3000
2	0.92	0.91	0.07	0.01	0.03	200
3	0.92	0.83	0.07	0.01	0.09	200
4	0.90	0.79	0.15	0.01	0.05	1000–5000
5	0.91	0.78	0.17	0.01	0.06	300–600
7	0.85	0.68	0.17	0.04	0.08	300
6[b]	0.63	0.69	0.08	0.08	0.17	300

Note. Values were determined by extrapolation to zero time on stream. Qualitative external/internal surface area ratios and *c*-direction crystallite lengths were determined from TEM data. Reaction conditions as stated in Table 3.

[a] Selectivity defined as mole fraction product component/mole fraction *n*-hexane converted to product; C_1–C_5 selectivity calculated on basis of moles of C_6.

[b] Sample 6 run at higher space velocity than other samples (Table 3).

time on stream. Catalyst Samples 6 and 7 were characterized by lower initial benzene selectivities, and these decreased during catalyst deactivation (e.g., by about 12% for Sample 7).

Each of the catalysts made from the relatively small zeolite LTL crystallites (Table 1) is characterized by initial selectivities for benzene formation that are less than that characterizing the catalyst provided by Miller (Sample 1); correspondingly, the former catalysts are characterized by hydrogenolysis selectivities greater than that of the Miller catalyst. Catalyst Sample 2 was closest in performance to that of the Miller catalyst (Sample 1), having only slightly lower initial selectivity for benzene formation (0.90 vs 0.92) and only a slightly higher initial selectivity for C_1–C_5 products (0.06 vs 0.04). The catalysts that deactivated the least (Samples 1, 2, and 3) were almost unchanged in selectivity over the full periods of operation. The benzene selectivities of Samples 4 and 5 decreased by 4 and 7%, respectively, over the course of operation, and that of Sample 7 decreased by 10% (Fig. 5A).

The initial *n*-hexane conversions, representing the performance of the undeactivated catalysts, are summarized in Table 4. These values are determined by extrapolation to zero time on stream of the data shown in Fig. 4A; the data representing the catalysts that underwent relatively rapid initial deactivation are characterized by larger uncertainties. Samples 1–5 are characterized by nearly the same initial total *n*-hexane conversion of 0.90–0.92. Sample 7 was significantly less active initially, with a total *n*-hexane conversion of 0.85.

The initial selectivity to each product, defined as the fraction of *n*-hexane converted to the product divided by the total conversion of *n*-hexane, extrapolated to zero on-stream time, is given in Table 4.

Rates of catalyst deactivation, determined both as an average of values, determined from data taken during the first 30 h on-stream and, alternatively, by differentiation of the data fitted with empirical curves and extrapolated to zero time on-stream, are summarized in Table 3. Catalyst Samples 1–3 underwent little deactivation, whereas Samples 4–7 underwent deactivation at substantial rates. Each of the three former samples is characterized by a high selectivity for benzene formation and by low selectivities for C_1–C_5 and for cyclohexane/MCP. Samples 1 and 2 also exhibited low selectivities for methylpentanes. The remainder of the catalysts are characterized by higher selectivities for these products; however, Sample 5 was exceptional, having a relatively high selectivity for C_1–C_5 products and a relatively low selectivity for cyclohexane/MCP and methylpentanes.

DISCUSSION

Comparison of Selectivities of Various Pt/LTL Zeolite Catalysts

A striking characteristic of the Pt/LTL zeolite catalysts that have found application is their high selectivities for formation of aromatic products. Thus, an important basis for comparison of the various samples of such catalysts is their selectivities for formation of benzene from *n*-hexane. Because the reaction network involves sequential reactions, with a number of the intermediates ultimately being converted into benzene (4), the selectivity is strongly dependent on conversion, and a satisfactory comparison of catalysts on the basis of selectivity requires data for each at the same conversion. Data characterizing the reported catalysts with the highest benzene selectivities are collected in Fig. 6; details of the catalysts and the reaction conditions are summarized in Table 5.

The most selective catalysts reported are all supported on nonacidic or almost nonacidic LTL zeolites and incorporate relatively small clusters of platinum. Of the most highly selective catalysts represented in Fig. 6, those that have been characterized by EXAFS spectroscopy (designated

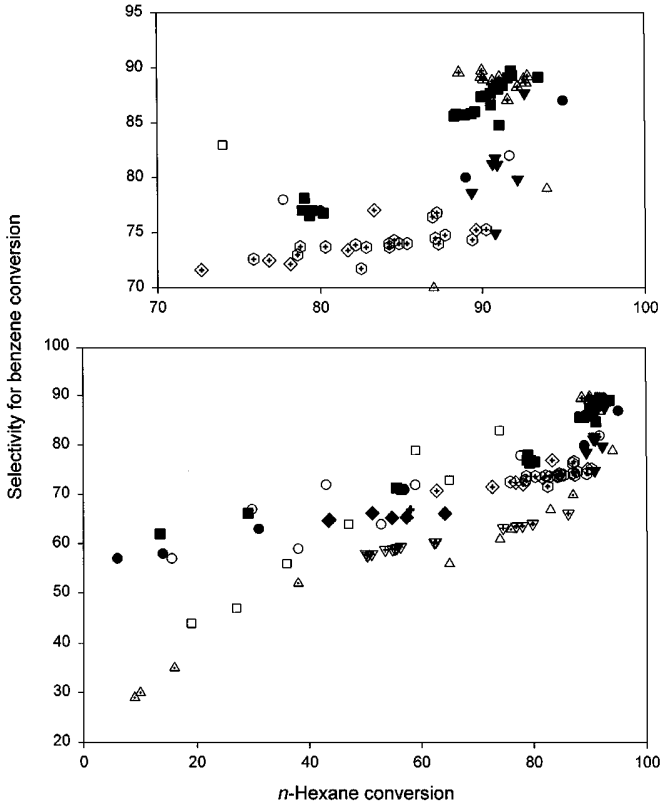

FIG. 6. Summary of selectivity data for benzene formed in *n*-hexane conversion catalyzed by Pt/KLTL zeolite. Selectivity defined as wt% benzene/wt% *n*-hexane converted to product. Closed symbols represent catalysts characterized by EXAFS, open symbols represent catalysts characterized using other techniques. Reaction conditions and catalysts given in Table 5. Symbols: ○, Mielcazrski *et al.* (9); □, Bernard (2); ●, Lane *et al.* (6); △, McVicker *et al.* (13); +, Tamm *et al.* (4); ■, Sample 1; ⟁, Sample 2; ▼, Sample 3; ⟐, Sample 4; ⊕, Sample 5; ◆, Sample 6; ⩛, Sample 7.

with closed symbols in Fig. 6) have been found to incorporate platinum clusters with average nuclearities less than *roughly* 20.

The data of Fig. 6 demonstrate that most of our catalysts are characterized by selectivities that are high, relative to those reported and approximately as high as the highest. The EXAFS data (Table 2) show that the catalysts reported here that have the highest selectivities also incorporate platinum clusters smaller than about 10 Å in average diameter (with nuclearities less than *roughly* 20). Thus, we conclude that some of our catalysts were well prepared; good preparation implies small platinum clusters on a nonacidic support.

Because the same catalyst preparation method was used to prepare Samples 2–7, we infer that the important differences from one of these catalyst samples to another are associated with differences in the zeolite particle morphologies. Our data provide the first opportunity to determine the effects of zeolite morphology and zeolite crystallite size on catalyst performance in *n*-hexane dehydrocyclization.

Lack of Effect of Zeolite Channel Length (Crystallite Length) on Catalytic Properties

EXAFS data were obtained for Samples 1, 3, and 6 (Table 2). The average platinum cluster sizes in these samples were all nearly the same. In the following paragraph, we compare the conversion, selectivity, and stability (resistance to deactivation) results characterizing these catalysts, using data taken at the same space velocity. The highest conversions, selectivities, and stabilities were observed for Samples 2 and 3, which are characterized by the smallest zeolite crystallite lengths (about 200 Å). Samples 4 and 5, with crystallite lengths of about 1000–5000 and 300–600 Å, respectively, showed almost the same (but slightly lower) initial *n*-hexane conversions (typically, 0.90 vs 0.92, Table 4). However, Samples 4 and 5 gave significantly lower benzene selectivities and higher rates of deactivation. Sample 7, with crystallite lengths similar to those of Samples 2 and 3 (200–300 Å), was the least active catalyst and the one with the lowest benzene selectivity and the highest rate of deactivation. The results give no evidence of a correlation between the zeolite crystallite length and conversion.

Thus, because the TEM data indicate nearly uniform distributions of platinum in the intracrystalline pores of these samples, the reaction results give no evidence of intracrystalline mass transfer influence. A practical conclusion following from this inference is that it does not appear to be feasible to improve on catalyst performance simply by the use of smaller zeolite crystallites.

Effect of Zeolite Morphology on Catalyst Performance

The TEM data show no preferential locations for the platinum clusters; neither the extracrystalline nor intracrystalline regions are favored. This observation, in combination with the wide range of extracrystalline to intracrystalline surface area ratios in the family of samples, allows us to infer that the catalysts with the higher extracrystalline to intracrystalline surface area ratios incorporate relatively large fractions of the platinum outside the intracrystalline pores. Reaction data show that the catalyst performance is dependent on this ratio (which is related to the zeolite morphology), as follows: in comparison with the others, the catalysts with the relatively low fractions of platinum outside the intracrystalline pores are more active (but only slightly, Fig. 4A), more selective for benzene formation (Fig. 5A), and more stable (and the differences are large, Fig. 4A). These observations are the central results of this work. Specifics follows.

Samples 2 and 3, made from the 200×1000 Å disk-shaped zeolite crystallites and having relatively small fractions of the platinum present outside the intracrystalline pores, were found to be the most active (Fig. 4A), selective for benzene formation (Fig. 5A), and resistant to deactivation (Fig. 4A), with the activity indicated by the initial conversion of *n*-hexane. The catalysts prepared from small

TABLE 5

Conditions and Catalyst Descriptions for Benzene Selectivity Data Presented in Fig. 6

Symbol	Ref.	Support	Preparation technique	Temperature, °C	Total pressure, atm	Hydrogen/ hydrocarbon ratio, molar
○	Mielczarski *et al.* (9)	KLTL zeolite	Vapor impregnation	460	1	6
□	Bernard *et al.* (2)	KLTL zeolite, Si/Al ratio = 2.7 (molar)	Incipient wetness with $Pt(NH_3)_4Cl_2$	460	1	6
●	Lane *et al.* (6)	KLTL zeolite, Si/Al ratio = 2.3 (molar)	Incipient wetness with $Pt(NH_3)_4(NO_3)_2$	420	1	7.8
△	McVicker *et al.* (13)[a]	KLTL zeolite with binder	Ion exchange	510	8.17	6
+	Tamm *et al.* (4)	KLTL zeolite	Incipient wetness with $Pt(NH_3)_4(NO_3)_2$	466	6.8	6
■, ◭, ▼, ◈, ⊕, ◆, ⩛[b]	This work	KLTL zeolite	Incipient wetness with $Pt(NH_3)_4(NO_3)_2$	420	1	7.8

[a] Feed conversion defined as 100 − (wt% *n*-hexane + wt% MCP).
[b] ■, Sample 1; ◭, Sample 2; ▼, Sample 3; ◈, Sample 4; ⊕, Sample 5; ◆, Sample 6; ⩛, Sample 7.

(200–300-Å long) mosaic crystallites (Samples 6 and 7) and having the largest fraction of the platinum clusters outside the intracrystalline pores show relatively low *n*-hexane conversions (Fig. 4A), relatively low benzene selectivities (Fig. 5A), and relatively rapid deactivation (Fig. 4A). The catalysts prepared from the larger (300–600-Å and 1000–5000-Å long) mosaic zeolite crystallites (Samples 5 and 4, respectively) and having intermediate fractions of the platinum clusters outside the intracrystalline pores gave relatively high *n*-hexane conversions (Fig. 4A), only slightly lower than those observed for Samples 2 and 3, which were prepared from the disk-like crystallites. However, Samples 4 and 5 showed significantly lower benzene selectivities than Sample 2 (Fig. 5A) and relatively rapid deactivation (Fig. 4A), similar to what was observed for Samples 6 and 7 (prepared from the small mosaic crystallites).

The data plotted in Figs. 6–8 summarize the selectivity as a function of conversion and show that the pattern is similar for both the fresh and the partially deactivated catalysts. There is no clearly discernible effect of the catalyst aging on the selectivity versus conversion plots that can be separated from the effect of decreasing total *n*-hexane conversion on the selectivity. Furthermore, the data of Figs. 7 and 8 are consistent with the reaction network of Tamm *et al.* (4), indicating the primary products (e.g., cyclohexane/MCP) and secondary products (e.g., methylpentane). The relatively low selectivities of Samples 4, 5, and 7 for benzene formation (Fig. 6) correspond to relatively high selectivities of these catalysts for hydrogenolysis (Table 4).

Thus, a key question appears to be the following: What explains the effect of the location of the platinum on the catalyst performance? We suggest some answers in the following paragraphs:

Why is the initial conversion lower for Samples 4, 5, and 7 than for Samples 2 and 3? Several possibilities are suggested:

- First, intracrystalline mass transfer might be considered to play a role, but, as stated above, the data weigh against this possibility.
- Second, the results might instead be accounted for by the suggestion that the platinum clusters outside the intracrystalline pores were larger than those in these pores, providing relatively less surface area for reaction than those in the intracrystalline pores and thus lower activity. The TEM data are not sufficient to confirm or rule out the suggestion that the platinum clusters outside the intracrystalline pores were significantly larger, on average, than those in the intracrystalline pores. Thus, this suggestion remains a possibility.

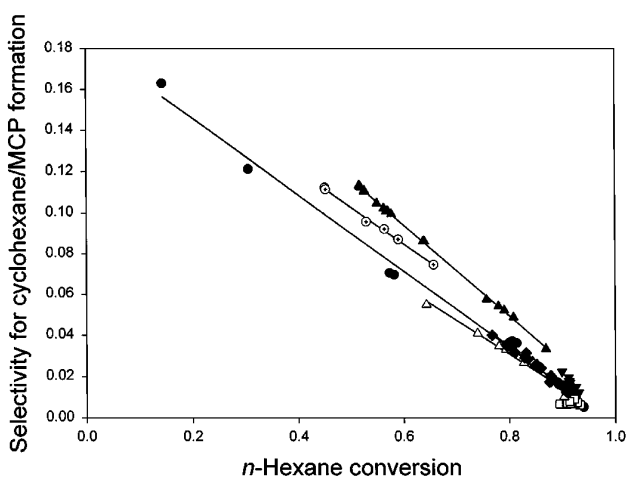

FIG. 7. Summary of selectivity data for primary products (cyclohexane/MCP) formed in *n*-hexane conversion catalyzed by Pt/KLTL zeolite samples at 420°C. Symbols: ●, Sample 1; □, Sample 2; ▼, Sample 3; ◆, Sample 4; △, Sample 5; ⊙, Sample 6; ▲, Sample 7.

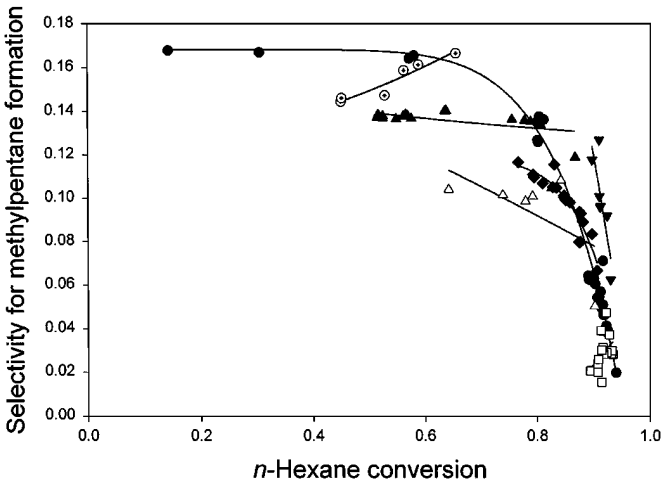

FIG. 8. Summary of selectivity data for secondary product methylpentane formed in *n*-hexane conversion catalyzed by Pt/KLTL zeolite at 420°C. Symbols: ●, Sample 1; □, Sample 2; ▼, Sample 3; ◆, Sample 4; △, Sample 5; ⊙, Sample 6; ▲, Sample 7.

• Third, because alkane hydrogenolysis is structure sensitive (31), the high initial hydrogenolysis activities of the catalysts with the relatively large fractions of the platinum outside the intracrystalline pores (Fig. 4C) might also be explained by the (unverified) suggestion that the platinum clusters outside the intracrystalline pores were relatively large.

• Fourth, we do not entirely rule out the possibility that, notwithstanding the consistency of the synthesis procedures used for all the catalyst samples, some of the samples may have retained some slight acidity. Thus, we should not rule out the possibility that the relatively high hydrogenolysis selectivities and correspondingly relatively low benzene selectivities observed for Samples 4, 5, and 7 might be associated with some residual acidity. However, we tend to discount this possibility because the measurements of acidity of KLTL zeolite samples (by ammonia desorption) reported by Mielczarski *et al.* (9) give no indication of residual acidic groups. Furthermore, we emphasize that the data representing Samples 4, 5, and 7 show that as the catalysts deactivated, both hydrogenolysis activity and benzene activity decreased, consistent with the loss of activity of platinum for both reactions.

The reaction data show that rate of catalyst deactivation also depends on zeolite particle morphology, as follows. Of the catalysts prepared in this work, Sample 2 exhibited the lowest rate of deactivation, the lowest ratio of extracrystalline to intracrystalline surface area, and the lowest initial hydrogenolysis selectivity. Catalyst Samples 4 and 5 exhibited higher rates of deactivation, intermediate extracrystalline to intracrystalline surface area ratios, and high selectivities for hydrogenolysis. Catalyst Sample 7 exhibited the highest rate of deactivation, the highest extracrystalline to intracrystalline surface area ratio, and a high selectivity for hydrogenolysis. Samples 4, 5, and 7, all characterized by high hydrogenolysis selectivities, underwent relatively rapid deactivation and rapidly lost hydrogenolysis selectivity (Fig. 4C). Thus, the rapid decrease in hydrogenolysis selectivity is correlated with the presence of platinum clusters outside the intracrystalline pores. Presumably, these extracrystalline clusters deactivate relatively fast.

Thus, the pattern of the deactivation data is broadly in agreement with the explanation of Iglesia and Baumgartner stated in the Introduction (7). However, our data are not sufficient to determine the validity of Iglesia and Baumgartner's suggestion that the extracrystalline platinum has the same initial selectivity as the intracrystalline platinum. Part of the difficulty regarding this issue may be related to the different conversions used in their work (<15%) and ours (>60% for fresh catalysts and >45% for those that had deactivated), the fact that they used *n*-heptane and not *n*-hexane as the hydrocarbon reactant, and the fact that we do not know how much our catalyst performance changed during the operation prior to the first product samplings.

TEM results indicate that the platinum shown by EXAFS spectroscopy to be highly dispersed on the fresh catalysts does not form significantly larger clusters or particles during deactivation and suggest that the zeolite stabilizes small platinum clusters, perhaps even those deposited on the external zeolite surfaces, which constitute a significant fraction of the total in some samples (e.g., Samples 6 and 7, Table 1). The premise of stabilization of platinum clusters on the external zeolite surfaces is consistent with the conclusion that these clusters are deactivated predominantly by coke formation (7) rather than aggregation and loss of platinum surface area.

In summary, we infer that there are intracrystalline and extracrystalline sites in the zeolite samples where small clusters of platinum are stably supported and that the platinum in the latter sites is susceptible to relatively rapid deactivation in the absence of sulfur, presumably by virtue of coke formation. The interpretation is consistent with that of Iglesia and Baumgartner (7), who compared the deactivation of silica-supported and LTL zeolite-supported platinum catalysts and concluded that the platinum in pores larger than the intracrystalline pores of LTL zeolite is not protected by the steric influence of these pores and is therefore susceptible to deactivation by coke formation. Furthermore, the platinum on the extracrystalline surface is more highly selective for hydrogenolysis, although the reason why is not evident from the data presented here.

Characteristics of Good n-Hexane Dehydrocyclization Catalysts

The data reported here confirm the established conclusions that good monofunctional *n*-hexane dehydrocyclization catalysts consist of small platinum clusters on nonacidic LTL zeolite supports. Furthermore, they show the

advantage of having a large fraction of the platinum within the intracrystalline pores.

SUMMARY

The morphology of the LTL zeolite support influences the activity, selectivity, and stability of LTL zeolite-supported platinum cluster catalysts, but the length of the zeolite crystallites (200–5000 Å) was found not to influence the catalyst performance. The most stable catalysts are found to be those with supports consisting of disks of zeolite crystallites, and the least stable are those with supports consisting of mosaic zeolite crystallites. There is a strong correlation between the extracrystalline to intracrystalline surface area ratio and the activity, selectivity, and stability of the catalysts. These data indicate that platinum in the intracrystalline zeolite pores and the platinum on the extracrystalline surfaces behave differently. Both the extracrystalline and intracrystalline surfaces stabilize small (on average, approximately 20-atom) clusters of platinum; the platinum on the external surfaces is deactivated more rapidly than that in the zeolite pores, consistent with the interpretation of Iglesia and Baumgartner (7), who postulated that the platinum within the zeolite pores is protected from deactivation by coke formation (a bimolecular reaction) by steric restrictions in the pores, whereas platinum on the extracrystalline surfaces is not.

A practical conclusion is that to synthesize a highly stable catalyst which is highly selective for benzene formation, the zeolite particles should be selected to have low values of the extracrystalline to intracrystalline surface area ratio, and the zeolite pore lengths may be as great as about 5000 Å without introduction of significant mass transfer limitations for conversion of *n*-hexane to benzene. The platinum clusters in the intracrystalline zeolite pores are more selective for benzene formation than those outside these pores, possibly because both hydrogenolysis and dehydrocyclization are structure-sensitive reactions.

ACKNOWLEDGMENTS

We thank J. T. Miller for supplying a catalyst sample. This research was supported by the U.S. Department of Energy, Office of Energy Research, Office of Basic Energy Sciences (grant number FG0287ER13790). We acknowledge beam time and the support of the U.S. Department of Energy, Division of Materials Sciences, under contract number DE-FG05-89ER45384, for its role in the operation and development of beam line X-11A at the National Synchrotron Light Source. The NSLS is supported by the Department of Energy, Division of Materials Sciences and Division of Chemical Sciences, under Contract No. DE-AC02-76CH00016. We are grateful to the staff of beam line X-11A for their assistance. The EXAFS data were analyzed with the XDAP software (23).

REFERENCES

1. Bernard, J. R., and Nury, J., U.S. Patent 4,104,320 to Elf France (1978).
2. Bernard, J. R., *in* "Proceedings of the Fifth International Zeolite Conference," (L. V. C. Rees, Ed.), p. 686. Heyden, London, 1980.
3. Hughes, T. R., Buss, W. C., Tamm, P. W., and Jacobson, R. L., *in* "Studies in Surface Science and Catalysis," Vol. 28, "New Developments in Zeolite Science and Technology" (Y. Murakami, A. Iijima, and J. W. Ward, Eds.), p. 725. Elsevier, Amsterdam, 1986.
4. Tamm, P. W., Mohr, D. H., and Wilson, C. R., *in* "Studies in Surface Science and Catalysis," Vol. 38, "Catalysis 1987" (J. W. Ward, Ed.), p. 335. Elsevier, Amsterdam, 1988.
5. Rotman, D., *Chem. Week* Feb. 26, 8 (1992).
6. Lane, G. S., Modica, F. S., and Miller, J. T., *J. Catal.* **129**, 145 (1991).
7. Iglesia, E., and Baumgartner, J. E., *in* "New Frontiers in Catalysis" (L. Guczi, F. Solymosi, and P. Tetenyi, Eds.), Studies in Surface Science and Catalysis, Vol. 75, p. 993. Elsevier, Amsterdam, 1993.
8. Davis, R. J., and Derouane, E. G., *Nature* **349**, 313 (1991).
9. Mielczarski, E., Hong, S. B., Davis, R. J., and Davis, M. E., *J. Catal.* **134**, 359 (1992).
10. Davis, R. J., *Heterogene. Chem. Rev.* **1**, 41 (1994).
11. Meriaudeau, P., and Naccache, C., *Catal. Rev. Sci. Eng.* **39**, 5 (1997).
12. Miller, J. T., Agrawal, N. G. B., Lane, G. S., and Modica, F. S., *J. Catal.* **163**, 106 (1996).
13. McVicker, G. B., Kao, J. L., Ziemiak, J. J., Gates, W. E., Robbins, J. L., Treacy, M. M. J., Rice, S. B., Vanderspurt, T. H., Cross, V. R., and Ghosh, A. K., *J. Catal.* **139**, 48 (1993).
14. Vaarkamp, M., Grondelle, J. V., Miller, J. T., Sadjkowski, D. J., Modica, F. S., Lane, G. S., Gates, B. C., and Koningsberger, D. C., *Catal. Lett.* **6**, 369 (1990).
15. Sharma, S. B., Ouraipryvan, P., Nair, H. A., Balaraman, P., Root, T. W., and Dumesic, J. A., *J. Catal.* **150**, 234 (1994).
16. Derouane, E. G., and Vanderveken, D. J., *Appl. Catal.* **45**, L15 (1988).
17. McVicker, G. B., Verduijn, J. P., Kao, J. L., Ziemiak, J. J., Treacy, M. M. J., Vanderspurt, T. H., and Gates, W. E., *in* "214th American Chemical Society National Meeting, Division of Petroleum Chemistry, Las Vegas, 1997."
18. Vaarkamp, M., Miller, J. T., Modica, F. S., Lane, G. S., and Koningsberger, D. C., *J. Catal.* **138**, 675 (1992).
19. Tsapatsis, M., Lovallo, M., Okubo, T., Davis, M. E., and Sadakata, M., *Chem. Mater.* **7**, 1734 (1995).
20. Jentoft, R. E., Deutsch, S. E., and Gates, B. C., *Rev. Sci. Instrum.* **67**, 2111 (1996).
21. Deutsch, S. E., Miller, J. T., Tomishige, K., Iwasawa, Y., and Gates, B. C., *J. Phys. Chem.* **100**, 13408 (1996).
22. Rehr, J. J., Mustre de Leon, J., Zabinsky, S. I., and Albers, R. C., *J. Am. Chem. Soc.* **113**, 5135 (1991).
23. Vaarkamp, M., Linders, J. C., and Koningsberger, D. C., *Physica B* **208/209**, 159 (1995).
24. Duivenvoorden, F. B. M., Koningsberger, D. C., Uh, Y. S., and Gates, B. C., *J. Am. Chem. Soc.* **108**, 6254 (1986).
25. Crozier, E. D., Rehr, J. J., and Ingalls, R., *in* "X-ray Absorption: Principles, Applications, Techniques of EXAFS, SEXAFS, and XANES" (D. C. Koningsberger and R. Prins, Eds.), p. 395. Wiley, New York, 1988.
26. Lovallo, M. C., and Tsapatsis, M., Nanocrystalline Zeolites, *in* "Advanced Catalysts and Nanostructured Materials" (W. R. Moser, Ed.), Chap. 13. Academic Press, San Diego, 1997.
27. Pan, M., *Micron* **27**, 219 (1996).
28. van Zon, J. B. A. D., Ph.D. dissertation, Eindhoven University of Technology, The Netherlands, 1988.
29. Vaarkamp, M., Modica, F. S., Miller, J. T., and Koningsberger, D. C., *J. Catal.* **144**, 611 (1993).
30. Miller, J. T., Agrawal, N. G. B., Lane, G. S., and Modica, F. S., *J. Catal.* **163**, 106 (1996).
31. Che, M., and Bennett, C. O., *in* "Advances in Catalysis" (D. D. Eley, H. Pines, and P. B. Weisz, Eds.), Vol. 36, p. 117. Academic Press, New York, 1989.